Journal of Materials Chemistry B

Accepted Manuscript

ROYAL SOCIETY OF CHEMISTRY

www.rsc.org/materialsB

Samarium doped glass-reinforced hydroxyapatite with enhanced osteoblastic performance and antibacterial properties for bone tissue regeneration

Diana Morais[a], Maria Ascensão Lopes[a], João Coelho[b], Maria Pia Ferraz[c], Pedro Gomes[d], Maria Helena Fernandes[d], Nandyala Sooraj Hussain[b*] and José Domingos Santos[a]

[a] CEMUC, Departamento de Engenharia Metalúrgica e Materiais, Faculdade de Engenharia, Universidade do Porto (FEUP), Rua Dr. Roberto Frias, Porto, Portugal.

[b] INESC Porto/Departamento de Física, Faculdade de Ciências, Universidade do Porto (FCUP), Rua do Campo Alegre, Porto, Portugal.

[c] CEBIMED - Centro de Estudos em Biomedicina, Faculdade de Ciências da Saúde, Universidade Fernando Pessoa (FCS-UFP), Porto, Portugal.

[d] Laboratory for Bone Metabolism and Regeneration - Faculdade de Medicina Dentária, Universidade do Porto (FMDUP), Rua Dr. Manuel Pereira da Silva, Porto, Portugal.

*Address Correspondence to Nandyala Sooraj Hussain, Ph.D.
INESC Porto/Departamento de Física, Faculdade de Ciências,
Universidade do Porto (FCUP), Rua do Campo Alegre, 687,
4169-007, Porto, Portugal.
Tel: +351-220402301, Fax: +351-222094050
Email: nandyala.sooraj@gmail.com

Abstract:

A novel bioactive bone substitute with improved osteoblastic performance and effective antibacterial activity was developed, using a completely new approach based on a samarium (Sm^{3+}) doped P_2O_5 glass-reinforced hydroxyapatite composites (GR-HA). The composites were prepared by adding 2.5% (w/w) of the P_2O_5 glass to 97.5% (w/w) of HA. Four composites were developed, i.e. one non-doped composite, and three Sm^{3+} doped composites prepared with the P_2O_5 glass containing 0.5, 1 and 2 (mol %) of Sm_2O_3. The composites were labeled as GR-HA_control, GR-HA_0.5Sm, GR-HA_1Sm and GR-HA_2Sm. The composites were physicochemical and mechanically characterized, namely performing SEM, EDS and XRD analysis and flexural bending strength (FBS) assessment. The incorporation of Sm^{3+} in GR-HA matrix resulted in the presence of a residual Sm^{3+} containing phase besides HA, β-TCP and α-TCP phases, increased surface hydrophilicity and slightly higher FBS. Sm^{3+} doped composites exhibited improved osteoblastic cell response, as evidenced by a better F-actin cytoskeleton organization and higher cell proliferation and expression of relevant osteoblastic genes. In addition, adhesion of *Staphylococcus aureus* and *Staphylococcus epidermidis* was greatly reduced on these composites. The improved osteoblastic behavior and the antibacterial effects were dependent on the amount of Samarium in the composite, being particularly evident in the composite with higher Sm^{3+} content. Therefore, the developed composite GR-HA_2Sm appears as a successful bone substitute with osteoconductive and antibacterial properties.

Key words: Samarium; Hydroxyapatite; Bioactive glass; Osteoblastic behavior, Bacterial adhesion.

1. Introduction

Lanthanide ions (Ln^{3+}) have similar ionic radii to Ca^{2+}, but because of the higher charge, they have a greater attraction for Ca^{2+} sites on biological molecules.[1-5] The high affinity of Ln^{3+} for bone has been known for decades, due to their ability to replace Ca ions in hydroxyapatite.[6] The presence of Ln^{3+} in HA crystal structure appears to affect the bone metabolism inducing changes in the bone composition, crystal size and lattice structure, as documented in experimental[7] and clinical[8] data. *In vitro* studies also reported evident effects on bone cells[9-17]. As a consequence, inclusion of these elements on the composition of calcium phosphate biomaterials for bone tissue regeneration has also been considered, and reported to induce promising changes in the physicochemical and biological profiles. Incorporated Ln^{3+} in HA matrix include (La^{3+})[19-21], (Y^{3+}) and (In^{3+})[19], (Sm^{3+}) and (Gd^{3+}) [22] and, also, in nanostructured HA, namely (Ce^{3+})[23] and (Ce^{3+}) and (Sm^{3+}).[24] HA and TCP lanthanum phosphate composites have also been reported.[25]

An important feature of lanthanides is their apparent antimicrobial properties. Several cerium salts display activity against a wide range of bacteria.[3,26] Thus, the incorporation of Ln^{3+} into a bone graft may represent a great advantage, as infection still remains a major complication in bone surgery.[27] Regarding this, antibacterial properties were reported for Ce^{3+} containing biomaterials, e.g. HA,[23] bioactive glass[28] and alginate-based hydrogels.[29]

Although naturally biocompatible, HA presents poorer mechanical properties than natural bone, which represents a concern at load bearing sites. To improve this, HA may be reinforced with the incorporation of a small percentage of a $CaO\text{-}P_2O_5$ based glass (GR-HA). The bioactive glass is a source of certain ions (e.g. F^-, Mg^{2+}, Na^+, Zn^{2+}, Mg^{2+}, SiO_4^{4-}, Sr^{2+}) and its presence in the HA matrix modulates the physicochemical and the biological properties of HA.[30-33] The $CaO\text{-}P_2O_5$ GR-HA composites present proven improved mechanical properties and enhanced bioactivity, as shown by *in vitro* and *in vivo* studies, compared to commonly used calcium phosphate materials.[34-38] A great advantage of these glasses is the possibility of incorporating key ions into their structure, endowing the resulting GR-HA with specific biological features. Taking this into account, the present work reports the preparation and characterization of novel Sm^{3+} doped GR-HA composites. Samarium was selected for several reasons. Clinically, Sm^{3+} is used already to target the bone tissue exhibiting an adequate safety profile[39] and, also, it appears not to affect the behavior of osteoblastic cells.[40] The influence of the presence of Sm^{3+} in a GR-HA was not previously addressed, neither the potential antibacterial properties of Sm^{3+} containing materials. As such,

Samarium oxide doped GR-HA composites were prepared with three lanthanide concentrations, and were characterized for the physicochemical profile and also for its osteoblastic cell response and antibacterial properties.

2. Experimental

2.1. Preparation of Samarium glasses and GR-HA composites

For the preparation of the samarium-containing glass reinforced hydroxyapatite composites, glasses with distinct samarium concentrations were fabricated and mixed with hydroxyapatite. Briefly, a series of four glass species, with different chemical compositions (mol%): (i) 15CaO-10Na_2O-10CaF_2-65P_2O_5-0Sm_2O_3, (ii) 15CaO-10Na_2O-10CaF_2-64.5P_2O_5-0.5Sm_2O_3, (iii) 15CaO-10Na_2O-10CaF_2-64P_2O_5-1Sm_2O_3 and (iv) 15CaO-10Na_2O-10CaF_2-63P_2O_5-2Sm_2O_3, labeled respectively as control, 0.5% Sm, 1% Sm and 2% Sm, were prepared. Glasses were processed by the mixture of $CaHPO_4$, P_2O_5, Na_2CO_3, CaF_2 and Sm_2O_3, that was following melted in disposable platinum crucibles, in an electric furnace at a temperature of 1000 ^oC, for 1 hour. Subsequently, glasses were milled in dry conditions (AS 200 digit, *Retsch*, Germany), and sieved to a granule size $\leq$ 75 μm.

Glass particles were used for the preparation of glass-reinforced hydroxyapatite composites (GR-HA) at a proportion of 2.5% (w/w) of glass and 97.5% (w/w) of hydroxyapatite (HA). Pure phase HA, according to the standard ISO/DIS 13779-3, was used. The prepared composites were labeled as GR-HA_control, GR-HA_0.5Sm, GR-HA_1Sm and GR-HA_2Sm, according to the composition of the added glass. In order to ensure a homogenous mixing, HA and glass powders were mixed for 3 h, in dry conditions, in a mixer (Turbula-T2F, *WAB*, Germany). The attained mixed powders were used to prepare disks by uniaxial pressing at 80 MPa. These were following sintered in a furnace (*Termolab*, Portugal), at 1300°C for 1 h, using a 2 ^oC/min heating rate, followed by natural cooling inside the furnace.

2.2. Physicochemical and mechanical characterization of GR-HA composites

Scanning electron microscopy (SEM) analysis was performed, using a *FEI Quanta 400 FEG ESEM* microscope, to analyze the microstructure and morphology of the composite materials. Samples were coated with gold/palladium particles, using a *SPI Sputter Coater*, prior to the analysis. The SEM images were acquired using either the secondary or the back-scattered

electrons mode. The elemental composition was evaluated by energy dispersive X-ray spectroscopy (EDS).

X-Ray diffraction (XRD) analysis were conducted on composite powdered samples, using a Siemens D 5000 diffractometer, with Cu-Kα radiation (λ=1.5418 Å). The scans were made in the range of 25-40^{o} (2θ), using a step size of 0.02^{o} and a count time of 2 sec/step.

Surface roughness was characterized by the arithmetic mean roughness (Ra) measurement of the composite samples, with an Etamic GMBH profilometer with diamond tip feeler. Data was recorded by a Hommel tester T8000 software - for a 4.8 mm scanning, a 0.8 mm cut-off distance and a constant scanning speed of 0.5mm/s were used. 5 samples of each composition were evaluated.

Contact angle analysis (θ) was performed in accordance with the sessile drop method, at room temperature and humidity, using an Axsymmetric Drop Shape Analysis–Profile (ADSA-P) software. Prior to the analysis, composite disks were polished with water sandpaper in the following order: P320, P500, P2500, washed with distillated water and dried overnight at 100 ^{o}C. Drops (4μl) of ultra-pure water were dispersed on the surface of each material through a micro syringe and the deposition, to estimate the contact angle (θ), was recorded in video. Five samples of each composition were evaluated and no more than 20 drops on each one.

In order to assess the apparent density ($\rho_{apparent}$) of the composite materials, the diameter, thickness and weight of 5 disks of each composite were measured. The densities of these materials have been measured using ethyl glycol as an immersion liquid by Archimedes' principle on a Mettler Toledo balance.

Mechanical properties of the composites were evaluated by the Flexural bending strength (FBS) test, which was performed by the concentric ring-on-ring method using the *Lloyd Lr30K* equipment and data obtained from the *Windap V1.6* software. The used concentric jig presented the following dimensions: 20 mm for the supporting radius and 10 mm for the loading radius. The test was done at a cross speed of 5 mm/min and the rupture modulus determined by Soltesz proposed equation 1, in which σ is the rupture modulus, F is the load,

v is the Poisson's ratio (0.28), t is the thickness of the disk, r_2 is the radius of the supporting ring, r_1 is the radius of the loading ring and r is the sample's radius.[41]

$$\sigma = \frac{3F(1+v)}{4\pi t^2}\left(1 + \ln\left(\frac{r_2}{r_1}\right) + \frac{1-v}{1+v}\frac{r_2^2 - r_1^2}{r^2}\right) \qquad (1)$$

Following, the Weibull statistics were applied to strength data in order to determine failure probability versus load levels. The Weibull modulus (m) of the composites was estimated by plotting the equation 2, in which P is the probability of failure estimated by the equation 3. In the later, j is the rank value ordered from the smallest to the largest and n is the number of samples submitted to the test (n=12).

$$\ln\left[\ln\left(\frac{1}{1-P}\right)\right] = m\ln(\sigma) - m\ln(\sigma_0) \qquad (2)$$

$$P = \frac{j-0.3}{n+0.4} \qquad (3)$$

2.3. Osteoblastic cell response

Human osteoblastic-like cells (MG63 cells, ATCC number CRL-1427™) were cultured in α-Minimal Essential Medium (α-MEM), supplemented with 10% fetal bovine serum, Penicillin (10 units/mL)/Streptomycin (10 µg/mL) and 2.5 µg.ml^{-1} fungizone, at 37ºC, in a humidified atmosphere of 5% CO_2 in air. For sub-culturing, the cell layer (at around 70-80% confluence) was detached with trypsin – EDTA solution (0.05% trypsin, 0.25% EDTA; 5 minutes, 37ºC), and the cell suspension was used in the cell response studies. Material samples were cultured for 1, 4 and 7 days, and the culture medium was changed twice a week. GR-HA was used as control. Cultured composites were observed by Confocal Laser Scanning Microscopy (CLSM) and SEM, and were evaluated for cell adhesion, viability/proliferation and expression of osteoblastic genes.

For CLSM assessment, material samples were fixed (3.7% paraformaldehyde, 15 min), permeabilized (0.1% triton in PBS, 5 min), and incubated with a solution of 10 mg/ml of BSA (Bovine Serum Albumin) with 1 µg/ml RNAse in PBS (1 h). Cell cytoskeleton filamentous actin (F-actin) was stained by treating the cells with 5 U/ml Alexa Fluor® 488-Phalloidin (*Invitrogen*, Spain) (20 min). Cultures were treated with 10 µg/ml propidium iodide (*Sigma-Aldrich*, St. Louis) (10 min) for cell nuclei labelling. Labelled cultures were

mounted in Vectashield® and examined in a Leica SP2 AOBS (Leica Microsystems) confocal laser scanning microscope.

For SEM observation, samples were fixed (1.5% glutaraldehyde in 0.14M sodium cacodylate buffer, pH=7.3, 10 min), dehydrated in graded alcohols, dried in hexamethyldisilazane (HMDS) solution in alcohol ranging from 50 % (V/V) to 100 % (V/V), sputter-coated with an Au/Pd thin film (SPI Module Sputter Coater equipment), and observed in a High resolution (Schottky) Environmental Scanning Electron Microscope (Quanta 400 FEG ESEM).

The MTT assay was used to evaluate cell viability/proliferation on the colonized material samples. MTT (0.5 mg/ml) was added to the medium, and cultures were incubated for 4 h at 37ºC. Following, the formazan salts were dissolved in DMSO and the absorbance (A) was determined at λ = 600 nm on an Elisa reader (Synergy HT, Biotek).

Cultures were assessed by RT-PCR, at day 7, for the expression of the housekeeping gene glycerol-3-phosphate dehydrogenase (GAPDH), and the osteoblastic genes Runt-related transcription factor 2 (Runx2), Collagen type I (COL1), Alkaline phosphatase (ALP), Bone morphogenetic protein- 2 (BMP-2), Osteocalcin (OC) and Osteoprotegerin (OPG). For that, RNA was extracted with Rneasy® Mini Kit (QIAGEN) according to manufacturer's instructions and was quantified by UV spectrophotometry at 260 nm. Half microgram of RNA was reverse transcribed and amplified (25 cycles) with the Titan One Tube RT-PCR System (Roche), with an annealing temperature of 55ºC. Table 1 shows the primers used in the RT-PCR analysis. After electrophoresis on a 1% (w/V) agarose gel, the bands were analysed by densitometry with ImageJ 1.41 software. Values were normalized to the corresponding GAPDH value of each experimental condition.

2.4. Bacterial adhesion on composites surface

The bacterial strains *Staphylococcus aureus* (ATCC 25923), *Staphylococcus epidermidis* (ATCC 35984/RP62A) and *Pseudomonas aeruginosa* were used in the bacterial adhesion assay. The colorimetric MTT assay, based in the reduction of 3-(4,5-dimethylthiazol-2-yl)-2,5-diphenyltetrasodium bromide) (MTT, *Sigma*, Germany) by viable bacteria to a purple insoluble formazan product, was used to assess bacterial adhesion.

A bacterial suspension (1 ml) containing $1.5x10^8$ CFU/ml, prepared in Mueller Hinton Broth Medium (MHB, *Liofichem*, Italy), was poured onto the surface of the composite disks (previously sterilized by ethylene oxide), placed in a 24-well culture plate. The material samples were incubated at 37 ^oC, without agitation, for 4 h. After, the medium was removed and the samples were transferred to a new 24-well plate to guarantee that just adhered bacteria remain on the surface of the material. Then, 1 ml of new medium and 100 µl of MTT (0.5 mg/ml) was added to each well. Samples were incubated for 4 h at 37 ºC, protected from direct light, the medium was removed, and the formazan crystals were dissolved in dimethyl sulphoxide (DMSO, *Panreac*, Spain). The absorbance was read at λ = 565 nm using a microplate reader *Awareness Technology STAT FAX 3200*.

2.5. Statistical analysis

Where adequately, experimental data were presented as mean ± SD (standard deviation). For quantitative assays, 5 samples were evaluated for each time point (n=5). For qualitative microscopy analysis, samples were evaluated in triplicates (n=3) and at least 10 images were randomly obtained from each sample. For RT-PCR analysis, three individual experiments were performed, each one with triplicate replicas.

Statistical analysis of data was performed using the one-way ANOVA test, using the software *SigmaStat 3.5*. The differences were considered to be significant at a level of $p<0.05$.

3. Results

3.1. Physicochemical and mechanical characterization of the composites

3.1.1. SEM and EDS analysis

Representative SEM micrographs (Fig.1) of the prepared composites were acquired using the secondary electrons mode and a high magnification (3000x). The composites' surface presented a similar morphology with a homogenous structure and a typical wide grain size distribution, which was observed for all the prepared compositions. Further, brighter particles have been detected in Sm-containing composites, particularly in the GR-HA_1Sm and GR-HA_2Sm formulations, which may substantiate the presence of Sm within the composites' matrix. Therefore, SEM/EDS characterization was performed in order to ascertain the presence of this element. A representative back scattered SEM image (Fig.2A) of the GR-HA_2Sm composite, in which a Sm containing phase can be detected, as shown by the

distinctively brighter particles, is presented. These particles show a good distribution throughout the material's matrix. EDS analysis of these structures confirmed the presence of Sm (Fig. 2B) and the obtained relative ratio of Sm, P and Ca was 0.49, 5.84 and 8.62 respectively, in full correspondence with the nominal composition.

3.1.2. XRD analysis

XRD analysis was performed to identify the crystalline phases present in the GR-HA composites. The obtained patterns (Fig. 3) and were analyzed according to the Joint Committee on Powder Diffractions Standards (JCPDS).[42] The peaks displayed in the plot correspond to the main peaks reported in JCPDS files for HA (JCPDS 72-1243), β-TCP (JCPDS 09-0169) and α-TCP (JCPDS 9-348). It should be noticed that the main peak attributed to HA is the most intense on GR-HA_2Sm, decreases progressively on GR-HA_1Sm and GR-HA_0.5Sm, and is the least intense on GR-HA_control. The peaks attributed to the TCP phases display a contrasting pattern, i.e. these are the least intense on GR-HA_2Sm, and increase in intensity in GR-HA_1Sm and GR-HA_0.5Sm, respectively, being the most intense on GR-HA_control. Additionally, the peaks that appear in the region around 28.2° for GR-HA_0.5Sm, GR-HA_1Sm and GR-HA_2Sm, may be explained by the presence of the new crystalline phase of samarium oxide (Sm_2O_3), once they match the peak with highest intensity described in ICDD 00-015-0813 file information of Sm_2O_3.

3.1.3. Surface roughness, contact angle and density evaluation

The surface roughness of all composites was estimated by Ra determination (Table 1). In comparison to control, Sm-containing composites presented a significant reduced Ra value, despite that, overall, all assayed compositions showed a microscale topography, ranging from around 4 to 6 μm. Also, Sm-containing composites presented significant lower contact angle values (ranging from around 61° to 71°), as comparing to the control composite (around 78°) (Table 1). The $\rho_{apparent}$ of all composites, geometrically calculated, strongly affects the mechanical properties of the materials and the results of this quantification are displayed in Table 1. As observed, despite the similarity among the values, the composite doped with the higher Sm concentration presents the higher $\rho_{apparent}$ value.

3.1.4. Flexural bending strength

The FBS tests (Fig.4) were performed to evaluate the probability of failure for all the developed composites under specific loads. Which presents the probability of failure versus the bending strength for each composite; it is possible to observe that Samarium doped composites presented higher values, in comparison to control. After applying the Weibull statistic to data, the *m* values for the materials were estimated, being around 3 and 4, for the control and Sm doped composites, respectively.

3.2. Osteoblastic cell response

3.2.1. Cell adhesion and pattern of cell growth

The cell adhesion process and the cell/biomaterial interactions were addressed by CLSM and SEM imaging. The characterization at early time points, i.e. 6 hours of culture, revealed no significant differences between developed composites, in terms of cell morphology, as adhered cells presented a broadly spherical morphology (data not shown).

CLSM images (Fig.5A) of the colonized composites at 1 day of culture showed that osteoblastic cells adhered to all surfaces and presented mostly an elongated morphology. At this culture time, cells established already cell-to-cell contact, and active cell division was also noticed. High magnification CLSM images (Fig.5B) showed some differences in the cell morphology and in the F-actin cytoskeleton organization, among the distinct composites. Over the GR-HA composite, cells presented low cytoplasm expansion, with the presence of groups of cells with rounded morphology and poor visibility of the nucleus. F-actin fibers presented diffuse distribution in the cytoplasm, and a higher density at the cell periphery. Over the Sm doped GR-HA higher cytoplasm expansion was evident, particularly on the composites with higher Sm content. Cells presented mostly elongated morphology with visible prominent nuclei, and well developed and organized F-action cytoskeleton as seen by the distribution of the stress fibers. SEM images (Fig.5C) revealed the presence of elongated cells, with filopodia, that were able to adapt to the underlying composite surface.

SEM observation (Fig. 6, Left) at day 7, showed a well-organized layer of elongated cells over all composites, which covered the material surface and presented a perfect adaptation to the composite topography. CLSM images at day 7, (Fig. 6, Right) provided the similar information, but in addition, cells stained intensively for the F-actin cytoskeleton and exhibited well-defined cell limits.

3.2.2 Cell viability/proliferation and expression of osteoblastic genes

The MTT assay (Fig.7A), revealed that cell viability/proliferation increased throughout the culture time over all composites. The Sm doped composites presented slightly higher values, ~20% at day 7, for the GR-HA_2Sm. The cell layer was assessed, at day 7, for the expression of some representative osteoblastic genes, i.e. Runx2, COL 1, ALP, BMP-2, OC and OPG. The Sm doped composites presented increased expression of Runx-2, ALP, BMP-2 and OC, (Fig.7B).

3.3. Bacterial adhesion

Results for the bacterial adhesion (Fig.8) to the composites' surface, evaluated after 4h culture time. Compared to the GR-HA composite, adhesion of both *Staphylococci* strains was greatly reduced in the Sm doped composites. Reduction was dependent on the Sm content. Adhesion of *P. areruginosa* was similar on GR-HA and the Sm doped composites.

4. Discussion

This study reported the preparation of Sm doped GR-HA composites, their physicochemical characterization, osteoblastic cell response and potential antibacterial properties.

SEM analysis of the developed composites (Fig. 1) revealed a characteristic homogenous structure, suggesting that the addition of Sm, in distinct amounts, did not modify the general microstructure of the prepared materials. It was also noticeable that the composites surface presented a wide range of grain sizes, which is a normal phenomenon after a sintering process.[43,44] The brighter points observed in the micrographs acquired in the back scattered mode (Fig. 2A) were attributed to a Sm containing phase, since this lanthanide has a much higher atomic number than calcium and phosphorous, being easily distinguished in the conducted SEM-EDS characterization. Furthermore, EDS evaluation of the referred particles revealed the presence of Sm within the calcium phosphate matrix (Fig. 2B), on all assayed Sm-containing compositions.

XRD analysis showed the presence of HA, β-TCP and α-TCP phases in all the preparations. It was expected that during the sintering process, due to the high temperatures, the added glasses became liquid and highly reactive, leading to the partial break down of HA, and to the consequent formation of secondary phases. In detail, HA matrix was transformed into β-TCP, which was then further transformed into α-TCP, as the glass entered HA's structure and

drove off the hydroxyl groups, altering the Ca:P ratio.[35,45] This is in agreement with reported results which confirm that, for a sintering temperature of 1300 ^{o}C, the referred phases of HA, β-TCP and α-TCP, can co-exist.[34,46] XRD analysis also revealed an increase in the HA phase percentage and a decrease in TCP phases percentage, particularly regarding β-TCP, as the Sm concentration increased in the GR-HA composition. This fact can be explained by the higher content of the new refractory Sm oxide phase, meaning that the doped glasses are less reactive than the control one, thus lessening the transformation of HA into β-TCP and α-TCP phases.[34,35,46]

The observed differences in phase composition also seem to influence the composites physicochemical properties. Accordingly, Sm-containing composites presented a surface roughness (Ra) value within the range of 4-4.5 μm, while the Ra of the control composite was around 6 μm. Despite the statistically significant differences, Ra values were found to be within the microscale topography range, previously shown to favour osteoblastic adhesion and to enhance cell proliferation and functional activity.[47] Developed composites also presented a contact angle (θ) value lower than 90^{o}, which sustains its hydrophilic behaviour.[48] Comparing to control, Sm-doped composites revealed significantly decreased θ values, and consequently, a more hydrophilic behaviour. This is in accordance with published data reporting that the lower the proportion of TCP phases within the composites' matrix, the more hydrophilic its behaviour would be.[48] Given that the addition of Sm reduced the proportion of TCP phases, the surface of Sm-doped composites was found to be more hydrophilic than the one verified in control. The distinct pattern of phase composition may also influence the biomechanical behaviour of the composites, as well as their the grain size and the porosity level.[35,45] The porous microstructure of a material strongly interferes with its mechanical behavior under stress. A high content of pores in a ceramic material decreases its mechanical strength, because they act as a stress concentration factor.[41,49] Thus, the higher $\rho_{apparent}$ of Sm doped composites (lower pores percentage) than of GR-HA_control (Table 1) can explain their higher resistance to fracture (higher FBS). It should be referred that the *m* values obtained for all the composites, as expected for ceramic materials, reflect a low reliability of the FBS, and therefore a difficult failure prediction. The phase composition of the doped composites is very similar to the non-doped composite, the only difference is the Sm_2O_3 phase. Once this phase is residual for all the doped composites, the slightly higher FBS (Fig. 4) obtained for these composites must be mainly due to a lower grain size and

porosity level. Also, it is worth to note, that the Sm incorporation in the calcium phosphate matrix caused an increase of materials $\rho_{apparent}$ values as the lanthanide concentration increases. This fact can be explained by the presence of Sm_2O_3 phase in all doped composites, which presents a higher ρ value than HA and TCP. However, this increase is very slight, probably due to the residual presence of Sm_2O_3 phase, and the $\rho_{apparent}$ values are lower than expected for these sintering materials, meaning a high porosity level. This can be related with some processing parameters, such as differences in HA and glass granules size, the used pressure and temperature to prepare the composites.

Sm doped composites were also characterized for the osteoblastic cell response, which was addressed for cell adhesion, F-actin cytoskeleton, proliferation and expression of relevant phenotype genes.

Observation of seeded cells during the first 24 h provided information on the cell adhesion to the composites' surface, namely on the cytoplasm expansion and the acquisition of the typical cell morphology, events that are strongly dependent on the reorganization of the F-actin cytoskeleton (Fig. 5A). Compared to the undoped GR-HA, there was a clear improvement in the cytoskeleton dynamics over the Sm doped composites. This effect was particularly noted in the composites with higher Sm amount, namely over GR-HA_2Sm, which displayed a better organization of the three-dimensional intracellular F-actin network. This is a relevant observation, as the F-actin cytoskeleton has a key role in the maintenance of the cell shape and cell junctions, gives mechanical support to cells and provides trafficking routes through the cytoplasm to aid signal transduction involved in intracellular transport, mitosis, cell motility and differentiation.[50,51] This structure also affects cell response to the extracellular environment, namely the cell adaptation to the surface topography.[51] Regarding this, cells proliferated throughout the culture time over all composites presenting an organized cell layer perfectly adapted to the surface topography (Fig. 6, Right).

Sm doped composites also showed an inductive effect on cell proliferation, and an up-regulation on the expression of Runx2, ALP, BMP-2 and OC (Fig. 7), genes typically related to osteoblastic differentiation.[52] These effects were also dependent on the amount of Sm in the composites, being significantly increased over GR-HA_2Sm. No literature information is available on the behavior of bone cells in samarium containing calcium phosphate based materials. However, it was reported that samarium oxide surfaces allowed normal adhesion

and proliferation of the human osteosarcoma cell line HOS cells.[40] In addition, the present results are also in line with that observed with other lanthanides. HA doped with La^{3+} promoted the adhesion, proliferation and differentiation of calvarial neonatal rat osteoblasts[28] and human osteoblasts.[19] Also, HA and TCP lanthanum phosphate composites allowed similar or improved adhesion of human osteoblasts, compared to the reference materials.[25]

The present and previous results are suggestive of the osteoblastic cytocompatibility of calcium phosphate materials containing lanthanides, and also support a trend for an improved cell behavior comparing to the reference materials. However, the mechanisms underlying the enhanced cell response over these materials are not fully elucidated. Nevertheless, the improved osteoblastic behavior might be related, at least partially, to the changes in the physicochemical profile induced by the presence of lanthanides in the HA matrix. Thus, in the present work, Sm doped composites presented some differences in the surface properties, compared to the undoped material, namely in the surface roughness and, more decisively, in the wettability values. Both parameters influence the type and the adsorption kinetics of the serum proteins to the materials' surface, events with a pivotal role in cell adhesion, morphology and migration.[53] In addition, the lanthanide itself is thought to play a role in the cell behavior. A variety of *in vitro* studies has reported that Ln^{3+} ions modulate the behavior of bone cells, by interfering with cell membrane bound mechanisms. There is evidence that these biological effects are due to the ability of Ln^{3+} ions to replace Ca ions in a variety of biological structures.[3,4] Accordingly, Ln^{3+} ions seem to interfere with the intracellular calcium $[Ca^{2+}]_i$ dynamics, namely by activating a membrane-bound Ca^{2+}-sensing receptor (CaR) or/and by blocking Ca^{2+}-dependent channels.[3,54] This is of utmost relevance, as calcium ions have a major role as a second messenger by modulating a variety of cellular functions,[55] and appropriate $[Ca^{2+}]_i$ seemed to favor osteoblastic proliferation and differentiation.[56] Also, there is a correlation between $[Ca^{2+}]_i$ and cytoskeleton organization, [57] and this mechanism might contribute to the better F-actin cytoskeleton organization seen in the present work over the Sm doped GR-HA composites, in line with that observed previously with La^{3+} in primary rat osteoblasts. [58]

The antibacterial properties of Sm doped GR-HA composites were evaluated against the main bacteria responsible for infections in hospital environment, namely in orthopedic surgical procedures, *S.aureus*, *S.epidermidis* (gram-positive bacteria) and *P.aeruginosa* (gram-

negative bacteria).[59] The used experimental protocol evaluated the bacterial adhesion on the composites' surface, in order to assess the ability of the materials in preventing biofilms formation. For *Staphylococci* strains, the bacterial adhesion decreased as the Sm concentration in the composite increased (Fig. 8). Differences in the hydrophilicity of reference and Sm doped composites might had a contribution to the lower adhesion on Sm composites, as it is known that both specific and non-specific bacteria/biomaterials interactions are greatly affected by this surface parameter.[27] Related to this, it has been reported that a decrease in the contact angle resulted in decreased adhesion of *S.aureus* and *S.epidermidis* in several surfaces.[27] Also, Sm might present antibacterial properties. Sm ions may be released from the composite matrix and disrupt bacterial membrane integrity affecting a variety of cellular processes such as adhesion, ion conductivity and cell signalling, as reported with other lanthanides like cerium.[29] In addition to the apparent effect on Staphylococcal adhesion, it is known that Ln ions inhibit Staphylococcal nuclease, a calcium-dependent secreted enzyme, due to their ability to replace Ca ions in biological molecules.[3] This enzyme degrades nucleic acids and participates in the *S. aureus* spread in the infected host, being considered an important factor of the microorganism pathogenicity. For *P.aeruginosa*, the presence of Sm does not prevent the bacteria adhesion, which agrees with studies reporting other lanthanides, namely cerium.[29,60] This behavior can be explained by the bacteria bacillus shape that allows the generation of more contact points with the material surface, enhancing the adhesion process. In addition, gram-negative bacteria present long, slender and flexible extensions, called pili, which have stronger adhesive properties than gram-positive bacteria, what also enhances the adhesion and makes the bacteria able to withstand higher physical stresses.[61] Moreover, besides the peptidoglycan layer, gram-negative bacteria presents a lipid external membrane containing lipopolysaccharides allowing a better interaction and adhesion with hydrophilic surfaces.[62] On the other hand, overall, gram-negative bacteria are less susceptible to biocides than gram-positive bacteria, because the presence of the lipid external membrane would difficult the contact of exogenous molecules with the cell membrane.

5. Conclusions

The incorporation of Sm in GR-HA matrix resulted in the presence of a residual Sm containing phase besides HA, β-TCP and α-TCP phases, as verified by SEM, EDS and XRD

analysis, and increased the surface hydrophilicity. Moreover, due to different physical properties, the doped composites presented a slightly higher FBS comparing to GR-HA_control. Sm doped composites exhibited improved osteoblastic cell response, as evidenced by a better F-actin cytoskeleton organization and higher cell proliferation and expression of relevant osteoblastic genes. In addition, adhesion of *S. aureus* and S. *epidermidis* was greatly reduced on these composites. The improved osteoblastic behavior and the antibacterial effects were dependent on the amount of Sm in the composite, being particularly evident in the composite with higher Sm content. Thus, the incorporation of Sm in the GR-HA matrix endowed the resulting composite with an enhanced osteoblastic cell response and an antibacterial activity, two key features contributing to a better outcome following bone graft implantation.

Acknowledgements

The authors would like to acknowledge the financial support from FCT (Fundação para a Ciência e a Tecnologia), through the project PTDC/SAU-BEB/103034/2008, and from the project ENMED/0002/ 2010, from FEDER funds through the program COMPETE-Programa Operacional Factores de Competitividade - under the project PEst-C/EME/UI0285/2011. Also, MHF and NSH would like to thank to e-cost ref. # MP 1301-New Generation Biomimetic and Customized Implants for Bone Engineering.

References

1. Monograph on *Physics and Chemistry of Rare-Earth ions doped Glasses,* ed. N. Sooraj Hussain and José Domingos Santos, Trans Tech Publishers, Switzerland, 2008.
2. Handbook on the *Physics and Chemistry of Rare Earths*, ed. K. A. Gschneidner, Jr and L. Eyring, Elsevier, USA, vol. 25, 1998.
3. S.P. Fricker, *Chem. Soc. Rev*., 2006, **35(6),** 524-533.
4. J. Zhang, Y. Li, X. Hao, Q. Zhang, K. Yang, L. Li, L. Ma, S. Wang, and X. Li, *Mini. Rev. Med. Chem*., 2011, **11(8),** 678-694.
5. M.E. Switzer, *Sci. Prog*., 1978, **65**, 19–30.
6. E. Pidcock and G.R. Moore, *J. Biol. Inorg. Chem.,* 2001, **6(5-6)**, 479-489.

7. J. Huang, T.L. Zhang, S.J. Xu, R.C. Li, K. Wang, J. Zhang and Y. N. Xie, *Calcif. Tissue Int*., 2006, **78,** 241-247.
8. M.H. Malluche, H. Mawad and M.C. Monier-Faugere, *Clin. J. Am. Soc. Nephrol*., 2008, **3 Suppl. 3,** S157-163.
9. L.D Quarles, J.E. Hartle, J.P. Middleton, J. Zhang, J. M. Arthur, and J.R. Raymond, *J. Cell Biochem.* 1994; **56(1),** 106-117.
10. J. C. Zhang, X. X. Li, S. J. Xu, K. Wang, S.F. Yu and Q. Lin, *Prog. Nat. Sci*., 2004, **14(4)**, 404-409.
11. J. Zhang, Y. Li, Q. Zhanz, X. Hao and S. Wang, *J. Rare Earths,* 2012, **30**, 831–834.
12. Z. Dawei, Z. Jinchao, C. Yao, Y. Mengsu and Y. Xinsheng, *Prog. Nat. Sci*. 2007, **17(5),** 618-623.
13. X. Wang, L. Yuan, J. Huang, T. L. Zhang and K. Wang, *J. Cell Biochem.,* 2008, **105(5),** 1307-1315.
14. J. Zhang, C. Liu, Y. Li, J. Sun, P. Wang, K. Di and Y. Zhao, *J. Rare Earths,* 2010;**28**,138-142.
15. J. Zhang, C. Liu, Y. Li, J. Sun, P. Wang, K. Di, H. Chen and Y. Zhao, *J. Rare Earths,* 2010, **28,** 466-470.
16. J. C. Zhang, T.L. Zhang, S.J. Xu, K. Wang , S.F. Yu and M.S. Yang, *J. Rare Earths,* 2004, **22(6**), 891-895
17. J.C. Zhang, T.L. Zhang, S.J. Xu, K. Wang , S.F. Yu and M.S. Yang, *J. Rare Earths,* 2005, **23(5),** 580-583.
18. C.A. Barta, K. Sachs-Barrable, J. Jia, K.H. Thompson, K.M. Wasan and C. Orvig, *Dalton Trans*., 2007, **43**, 5019-5030.
19. T. J. Webster, E.A. Massa-Schlueter, J.L. Smith and E. B. Slamovich, *Biomaterials,* 2004, **25,** 2111-2121.
20. D. G. Guo, A. H. Wang, Y. Han and K.W. Xu, *Acta Biomater*., 2009, **5(9)**, 3512-3523.
21. M.I. Ahymah Joshy, K. Elayaraja , R.V. Suganthi, V. Sarath Chandra and K.S. Narayana, *Curr. Appl. Phys.* 2011, **11(4),**1100-1106.
22. E.I. Get'man, S.N. Loboda, T.V. Tkachenko, N.V. Yablochkova, and K. A. Chebyshev, *Russ. J. Inorg. Chem.,* 2010, **55 (3),** 333-338
23. Y. Lin, Z. Yang and J. Cheng, *J. Rare Earths,* 2007, **25(4)**, 452-456.
24. I. Bogdanoviciene, M, Misevicius, A.Kareiva, K.A. Gross, T.C. K Yang, G.T. Pan, H.W. Fang and J.C. Yang, *Adv. Sci. Technol*, 2013, **86,** 22-27.

25. C. Ergun, H. Liu and T. J. Webster, *J Biomed Mater Res A.,* 2009, 89(3), 727-733.
26. L. Cobrado, M. M. Azevedo, A. Silva-Dias, J.P. Ramos, C. Pina-Vaz and A.G. Rodrigues, *J. Antimicrob. Chemother.*, 2012. **67 (5),** 1159-1162.
27. M. Katsikogianni and Y. F. Missirlis, Eur. *Cell* Mater., 2004, **8**, 37-57.
28. Y. Goh, A. Alshemary, M. Akram, M. Kadir and R. Hussain, *Ceram Int.,* 2014,**40**, 729-737.
29. D.S. Morais, M.A. Rodrigues, M.A. Lopes, M.J. Coelho,A.C. Maurício, R. Gomes, I. Amorim , M.P. Ferraz, J.D. Santos and C.M. Botelho, *J. Mater. Sci. Mater. Med*., 2013, **24,** 2145-2155.
30. S. Sprio, A. Tampieri, G. Celotti and E. Landi, *J. Mech. Behav. Biomed. Mater*., 2009, **2(2)**, 147-155.
31. R. Ravarian, F. Moztarzadeh , M.S. Hashjin, S.M. Rabiee, P. Khoshakhlagh and M. Tahriri, *Ceram Int.,* 2010, **36(1),** 291-297.
32. P.S. Gomes, C. Botelho, J. D. Santos and M.H. Fernandes, *J. Biomed. Mater. Res. Appl. Biomater*., 2010, **94B,** 337-346.
33. J. Coelho, N.S. Hussian , P.S. Gomes, P. Sampaio M. A. Lopes, M.H. Fernandes, J. D. Santos, *J. Am. Ceram. Soc*., 2012, **95**, 2732–2740.
34. M. A. Lopes, F. J. Monteiro and J. D. Santos, *Biomaterials,* 1999, **20,** 2085-2090.
35. M. A. Lopes, F. J. Monteiro and J. D. Santos, *J. Biomed. Mater. Res. A,* 1999, **48**(5), 734-740.
36. M. Gutierres, M.A. Lopes , N.S. Hussian, A.F. Lemos, J.M.F. Ferreira,A. Afonso, A.T. Cabral , L. Almeida and J.D. Santos,. *Acta Biomater*., 2008, **4**, 370-377.
37. S. Miao, N. Lin, K. Cheng, D. Yang, X. Huang, G. Han, W. Weng and Z. Ye, *J Am. Ceram. Soc*., 2011, **94,** 255-260.
38. A. Hoppe, N.S. Güldal, and A.R. Boccaccini ,*Biomaterials,* 2011, **32,** 2757-2774.
39. P.M. Anderson, G.A. Wiseman, A. Dispenzieri, C.A.S. Arndt, L.C.Hartmann, W.A. Smithson,B.P. Mullan and O.S. Bruland, *J. Clin. Oncol.,* 2002, **20,**189-196.
40. H.M.T.U. Herath, L. Di Silvio and J.R.G. Evans, *J. Biomed. Mater. Res. A.,* 2010, **94**(1), 130-136.
41. M.H.P. Silva, A.F. Lemos, J.M.F.Ferreira and J. D. Santos, *Mater. Res*., 2003, **6(3),** 321-325.
42. The International Centre for Diffraction Data, http://www.icdd.com/, (accessed November 2013).
43. P.V. Giannoudis , H. Dinopoulos and E. Tsiridis, *Injury*, 2005. **36**(3), 20-27.

44. A.R. Vaccaro, *Orthop*, 2002, **25**, 571-578.
45. J. C. Knowles, S. Tatal and J.D. Santos, *Biomaterials,* 1996, **17(14),** 1437-1442.
46. N. Sooraj Hussain, C.M Botelho, M. A. Lopes, M. Santos, J. V. Lobato, R.M,. Pinto, M. Gutierres and J. D. Santos, in *Biomaterials for Bone Regenerative Medicine,ed, N. Sooraj Hussain and J.D. Santos,* Trans Tech Publishers, Switzerland , 2009, Ch.6, pp. 153-180.
47. K. Anselme, A. Ponche, and M. Bigerelle , *Proc. Inst. Mech. Eng. H J. Eng. Med.,* 2010, **224**, 1487-1507.
48. M. A. Lopes, F. J. Monteiro and J.D. Santos, A.P. Serro and B. Saramago, *J. Biomed. Mater. Res.*, 1999, **45(4)**, 370-375.
49. M. A. Lopes, Ph.D. Thesis, University of Porto, 1999.
50. J. Stricker, T. Falzone and M. L. Gardel, *J. Biomech*., 2010, **43(1)**, 9-14.
51. F. Huber, J. Schnauss, S. Roenicke, P. Rauch, K. Mueller, C. Fuetterer and J. Kaes, *Adv. Phys.,* 2013, **62 (1),** 1–112.
52. J. Aubin, in *Principles of Bone Biology*, ed. J.P. Bilezikian, L.G. Raisz and T.J. Martin, Academic Press, 2008, pp. 85-107.
53. C.J. Wilson, R.E. Clegg, D.I. Leavesley and. M. J. Pearcy, *Tissue Eng.,* 2005,**11,** 1-18.
54. D. Riccardi, B. A. Finney, W. Wilkinson and P.J. Kemp, *Pflugers Arch*., 2009, **458(6),**1007-10022.
55. D.E. Clapham, *Cell,* 2007, **131(6),** 1047-1058.
56. S. Sun, Y. Liu, S. Lipsky and M. Cho, *FASEB J.,* 2007, **21(7)**,1472-1480.
57. I. Titushkin and M. Cho, *Biophy. J.*, 2007, **93(10),** 3693-3702.
58. X. Wang , J. Huang, T. Zhang and K. Wang, *Prog. Nat. Sci*., 2009, **19**, 331–335.
59. D. Campoccia, L. Montanaro and C. R. Arciola, *Biomaterials,* 2006, **27**, 2331-2339.
60. G.G. Gracia, *Burns,* 2001,**27,** 67-74.
61. T. Proft and E.N. Baker, *Cell. Mol. Life Sci.,* 2009, **66**, 613-635.
62. E.A. Araújo, N. J. Andrade, A.F. Carvalho, A.M. Ramos and C.A. Silva, *Química Nova*, 2010, **33**,1940-1948.

Table 1: Surface roughness, contact angle and apparent density of the prepared composites. *Significantly different from control (p<0.05).

Composite material	Ra (μm)	Θ (^{o})	$\rho_{apparent}$ (g/cm^3)
GR-HA_control	5.9 ± 0.66	78.3 ± 1.23	2.2±0.01
GR-HA_0.5Sm	4.6 ± 0.26 *	71.1 ± 1.07 *	2.3±0.03
GR-HA_1Sm	4.0 ± 0.24 *	65.5 ± 1.31 *	2.4±0.02
GR-HA_2Sm	3.9 ± 0.32 *	61.7 ± 1.22 *	2.5±0.01

Table 2: Primers used on RT-PCR analysis.

Gene	Forward primer	Reverse primer
GAPDH	CAGGACCAGGTTCACCAACAAGT	GTGGCAGTGATGGCATGGACTGT
Runx2	CAGTTCCCAAGCATTTCATCC	TCAATATGGTCGCCAAACAG
COL1	TCCGGCTCCTGCTCCTCTTA	ACCAGCAGGACCAGCATCTC
ALP	ACGTGGCTAAGAATGTCATC	CTGGTAGGCGATGTCCTTA
BMP-2	GCAATGGCCTTATCTGTGAC	GCAATGGCCTTATCTGTGAC
OC	CACTCCTCGCCCTATTG	CCCACAGATTCCTCTTCT
OPG	AAGGAGCTGCAGTAGGTCAA	CTGCTCGAAGGTGAGGTTAG

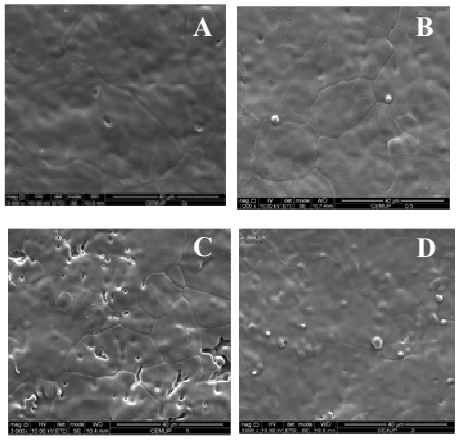

Fig. 1. Representative SEM micrographs of the prepared composites' surface. A - GR-HA_control; B - GR-HA_0.5Sm; C - GR-HA_1Sm; D - GR-HA_2Sm (High magnification X3000).

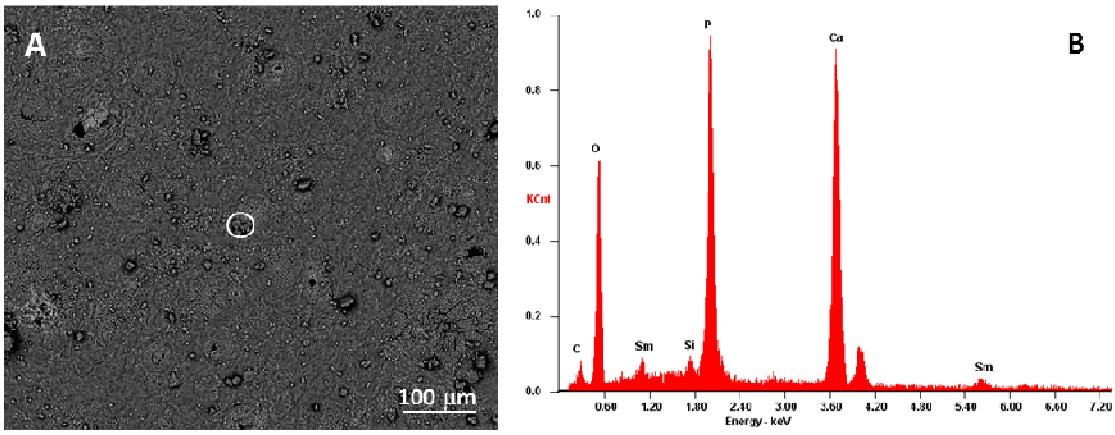

Fig. 2: (A) – Representative SEM back scattered image of GR-HA_2Sm surface, revealing the Sm distribution within the calcium phosphate matrix. Scale bar corresponds to 100µm. (B) EDS spectrum of the highlighted region in Fig. 2 (A).

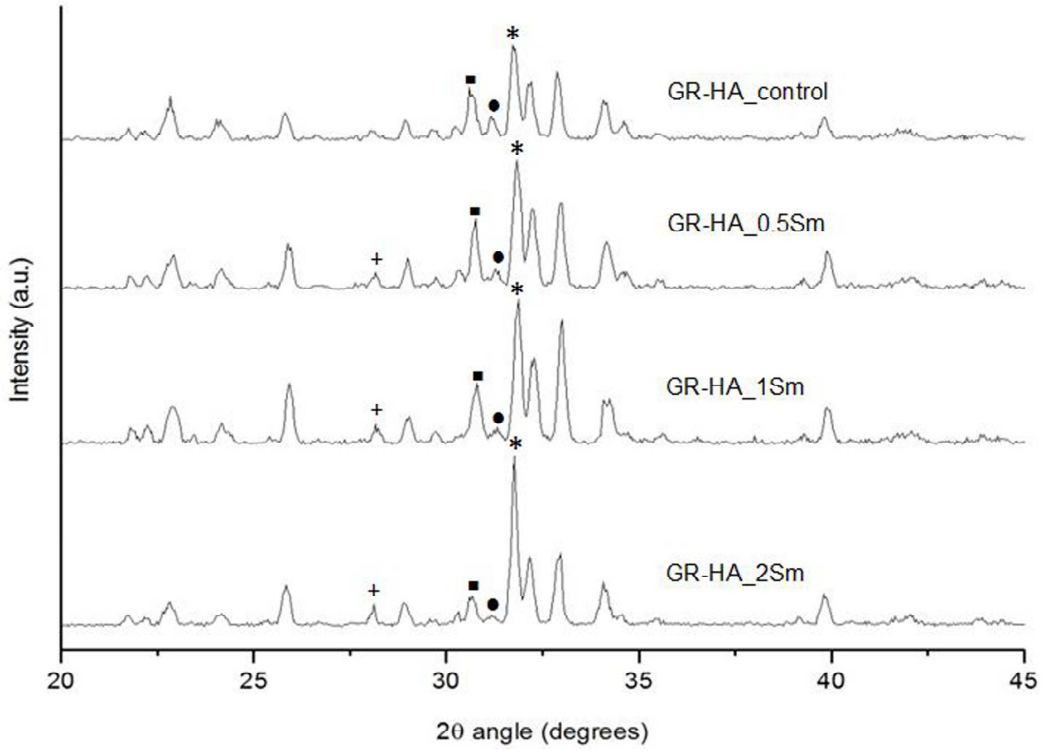

Fig. 3: XRD spectra of the prepared composites, showing the main peaks of each identified phase: * - HA; ● - β-TCP; ■ - α-TCP; + - Sm_2O_3.

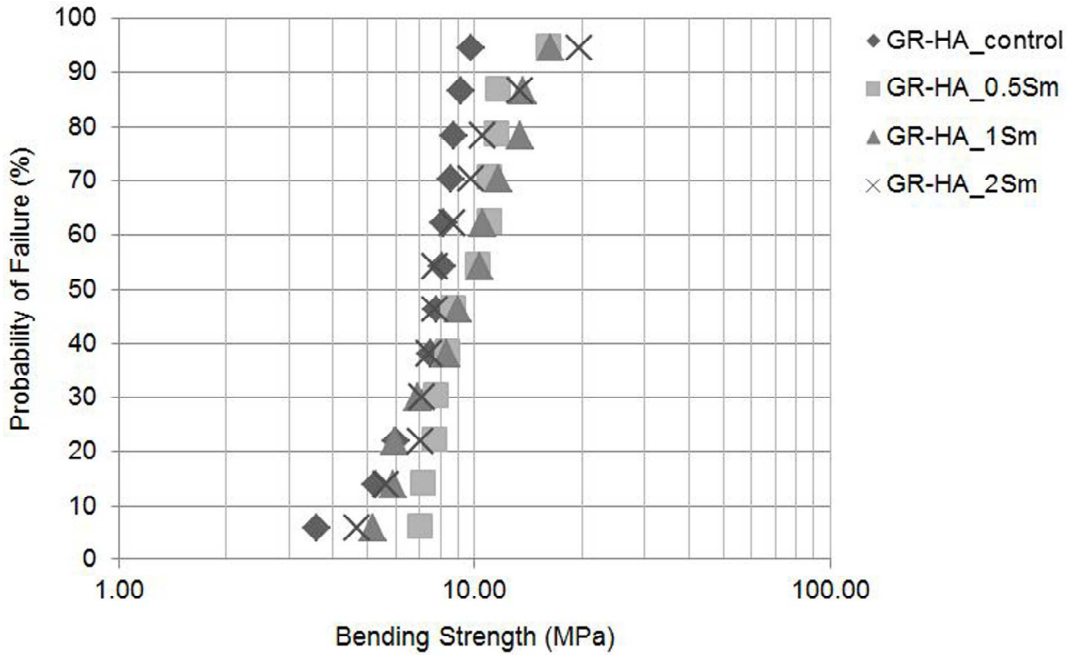

Fig. 4: Graphical representation of the Probability of failure vs. bending strength of the developed composites.

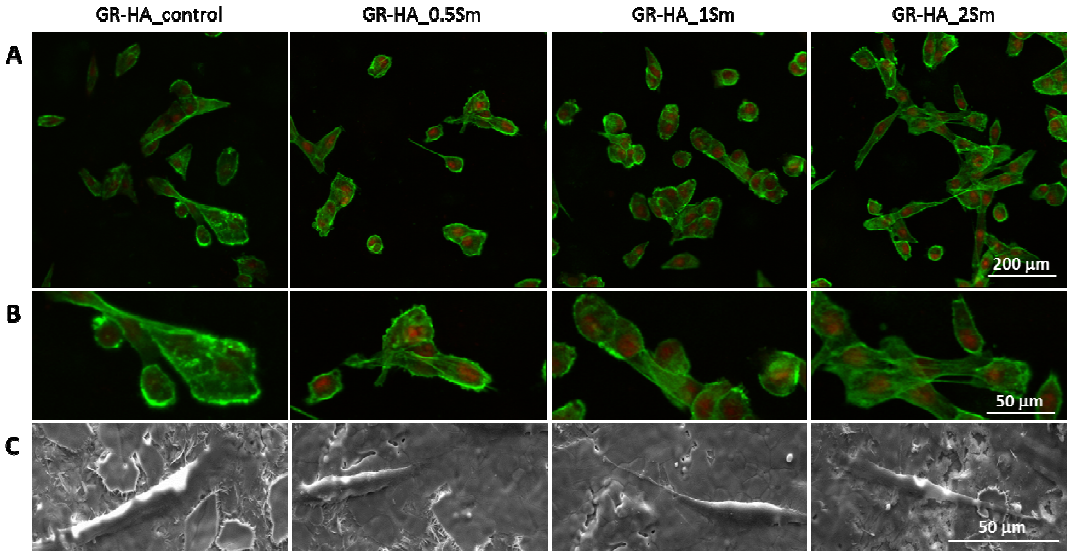

Fig. 5: Cell adhesion of MG63 osteoblastic cells seeded over GR-HA and Sm doped GR-HA composites, at 1 day of culture. Representative low (A), and high (B) confocal laser scanning microscopy images of cells stained for F-actin cytoskeleton (green) and nuclei (red); (C) representative scanning electron microscopy images.

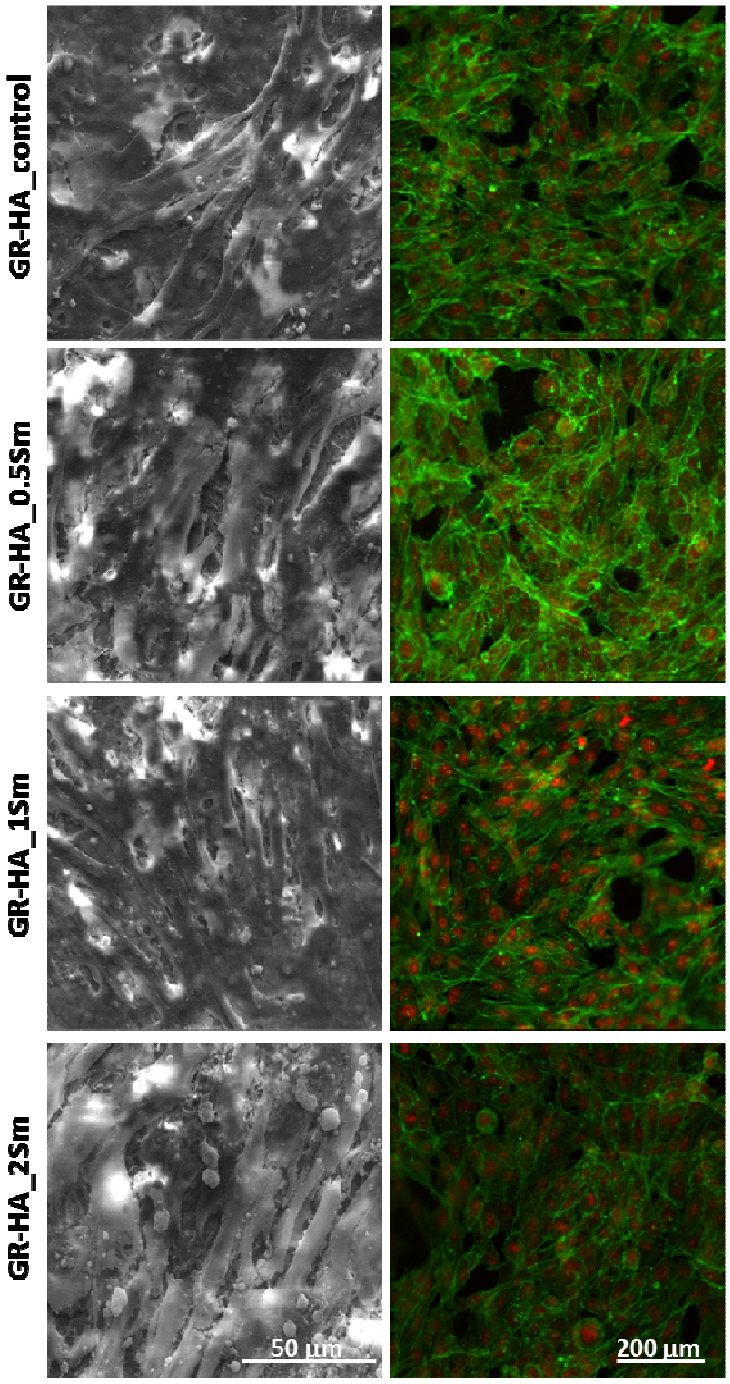

Fig. 6: Pattern of cell growth of MG63 osteoblastic cells cultured over GR-HA and Sm doped GR-HA composites, at day 7. (A) Scanning electron microscopy images (Left) and (B) confocal laser scanning microscopy images (Right).

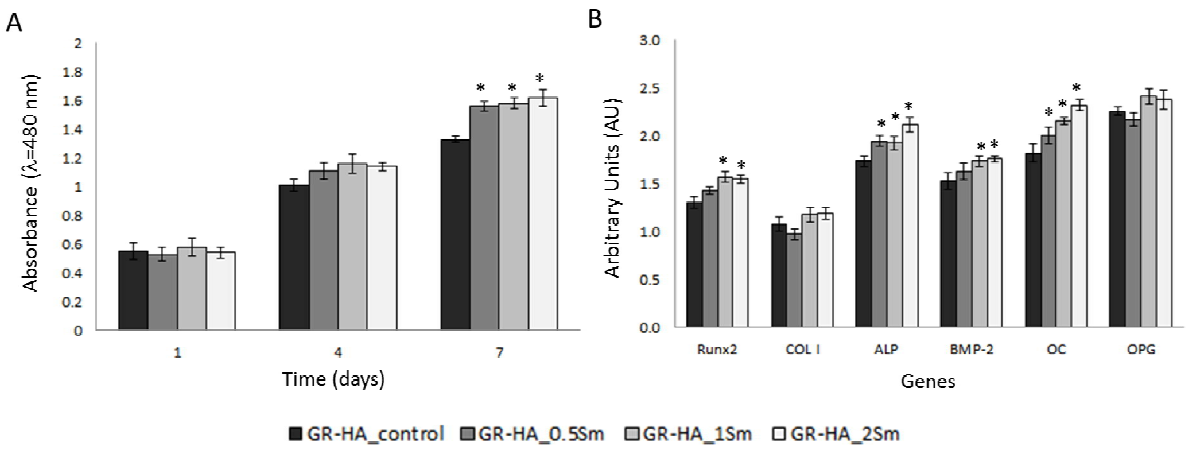

Fig. 7: (A) Cell viability/proliferation of MG63 osteoblastic cells seeded over GR-HA and Sm doped GR-HA composites, and cultured for 7 days. (B) Expression of the osteoblastic genes Runx2, Col 1, ALP, BMP-2, OC and OPG, at day 7. *Significantly different from control (GR-HA); $p \leq 0.5$.

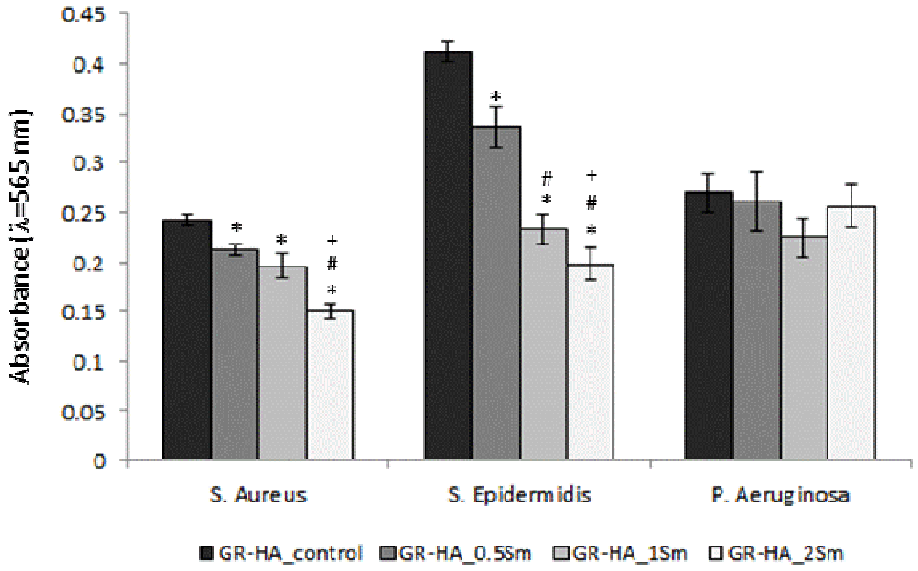

Fig. 8: Bacterial adhesion over GR-HA and Sm doped GR-HA composites after 4 h of incubation. *, significantly different from GR-HA_control; #, significantly different from GR-HA_0.5Sm; +, significantly different from GR-HA_1Sm (p<0.05).